International Journal of Solids and Structures 41 (2004) 4731–4755

INTERNATIONAL JOURNAL OF SOLIDS and STRUCTURES

www.elsevier.com/locate/ijsolstr

Continuum damage mechanics applied to paper

P. Isaksson [a,*], R. Hägglund [b], P. Gradin [a]

[a] Solid Mechanics, Mid Sweden University, SE-851 70 Sundsvall, Sweden
[b] SCA Packaging Research, Box 716, SE-851 21 Sundsvall, Sweden

Received 25 June 2003; received in revised form 27 January 2004
Available online 12 April 2004

Abstract

The mechanical behavior of two packaging paper materials subjected to tensile loading up to complete breakage has been investigated. A model for isotropic strain hardening elastic anisotropic plasticity, coupled to anisotropic damage, is discussed. The constitutive relations, including a gradient enhanced damage model, are developed within a thermodynamical framework. The Helmholtz free energy in the continuum is assumed to depend not only on the strain and stress components but also on the damage in the material.

The model has been analyzed in a non-linear finite element procedure. The capability of the model to properly capture and simulate the failure of a paper material subjected to tensile loading is demonstrated by means of several numerical examples that are compared to, and verified with, experiments on packaging paper specimens of varying geometry.

Keywords: Continuum damage mechanics; Plasticity; Paper material

---

1. Introduction

Packaging paper is the generic name for various types of paper used for packaging goods. The material known as corrugated board is made by a conversion process in which three or more layers of paper are laminated together. Corrugated cases are the cases manufactured from corrugated board sheets. Corrugated cases are principally used for transport packaging, as distinct from consumer packaging. The middle ply, which is called fluting, is corrugated during the process and the outer layers, called the liners, are glued to the peaks of the middle ply, thus making a liner-fluting-liner sandwich. The resulting structure is light but strong, with particular resistance to edge-wise compressive loading applied perpendicular to the manufacturing direction. This property gives the finished case a high "stacking strength". Packaging paper consists of a network of short cellulose fibres and is usually made by dewatering a cellulose fibre suspension on a wire. The fibres have an inherent capability to form bonds between them without any additives.

---

[*] Corresponding author.
E-mail address: per.isaksson@mh.se (P. Isaksson).

doi:10.1016/j.ijsolstr.2004.02.043

During manufacturing, the fibres tend to align themselves in the running direction of the wire and consequently bonded somewhat side-by-side in the cross-direction of the paper web. At a macroscopic level the material is often approximated as being orthotropic, i.e. having three mutually perpendicular planes of symmetry. The principal directions of material symmetry of paper are defined as machine direction (MD), which is the direction along the running web, cross-direction (CD), perpendicular to MD cross the web and the thickness direction (Z), Fig. 1.

Kraftliner and *Testliner* are the two main categories of liner materials. Kraftliner is a high-strength paper, made mainly from unbleached or bleached sulfate pulp. Testliner is made entirely from recycled fibres and was introduced originally as a substitute for Kraftliner. Fig. 2 shows SEM-photographs of the fibre network in the two materials.

When using acoustic emission monitoring (cf. Gradin et al., 1997) during uniaxial tensile testing of a paper specimen it is observed that stress waves start to emit at quite an early stage of loading. The source of these stress waves is believed to be the rapid relaxation of stresses close to a small fracture site, e.g. at a fibre/fibre bond or at a fibre. When the density of these fracture sites becomes significant, they will affect the mechanical properties of the paper. This is the motivation for applying what is commonly referred to as continuum damage mechanics on a paper material.

In continuum damage mechanics, the influence of damage on the mechanical properties is assumed represented by a set of continuous internal variables. The basic idea in continuum damage mechanics is that material degradation, or damage, can be described in a ‘‘smeared out’’ sense. Historically this idea dates back to a paper by Kachanov (1958) where creep rupture in terms of a continuously growing damage parameter was discussed. In recent years, the concept of damage mechanics has been extended to anisotropic materials. Isotropic damage is referred to the situation where the degradation of the elastic stiffness tensor depends on a single parameter and the damage growth rate also depends on a single parameter. For a generally anisotropic damage representation, a forth-rank damage tensor (cf. Lemaitre and Chaboche, 1990) has to be invoked.

It is possible to identify at least two damage processes for paper materials, e.g. fibre/fibre bond failure and fibre breakage. Generally, if it is assumed that both these processes are possible, it is necessary to include one set of damage variables (probably entirely different in both number and nature) for each process and also different criteria for onset of damage and different evolution laws. In this study it is assumed that there is one dominating damage process during tensile loading of a paper structure, even though there is nothing assumed about the nature of the actual damage process.

During acoustic emission monitoring of a paper specimen it is possible to get an approximate picture of the distribution of acoustic events along the length of the specimen. At some point the damage growth (acoustic events) will localize to a narrow band. If the conditions are such that this localization will not lead to unstable rupture, the specimen will exhibit a smooth descending load–elongation curve.

In experiments it has been observed that before the onset of acoustic emission (damage growth), the stress strain curve will deviate from linear behavior and upon unloading there will be a permanent deformation. One will, in addition to damage growth, also have another irreversible process commonly (but

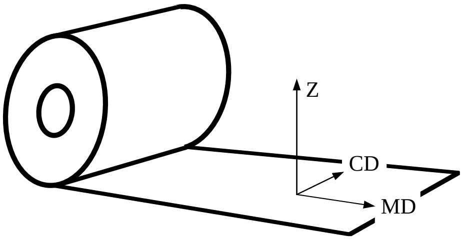

Fig. 1. The principal directions of material symmetry in paper.

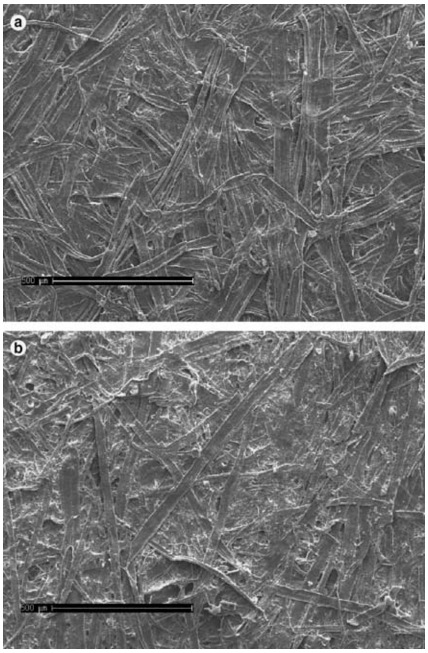

Fig. 2. Fibre network of Kraftliner (a) and Testliner (b). The magnification of the samples is 80× and the length indicator in the black area corresponds to 0.5 mm.

perhaps not correctly in this context) referred to as plasticity. One should have in mind that the mechanical processes on a micro-level in paper are different from those in, say, ductile metals. However, in order to avoid confusion, these processes are within this investigation referred to as plasticity processes.

The initial yield stress in MD is often different from that in CD and from Z. It has further been observed that paper materials show rather strong direction dependence also regarding the damage behavior as the onset of damage growth under continued tensile loading in MD is generally different from that in CD and from Z. In order to get a realistic description of the mechanical behavior of a mechanically loaded paper structure one have to combine an anisotropic model for damage evolution and an anisotropic model for plasticity.

The aim of this investigation has been to evaluate the applicability of the concept of continuum damage mechanics for analysis of packaging paper in tension. It is well known that paper materials behaves differently when loaded in compression than in tension. Analysis of a compressive loading situation is a subject of a forthcoming study.

The present investigation includes identification of a suitable constitutive model for the considered materials and implementation of a numerical scheme arising in the solution of the boundary value problem. In addition, mechanical testing of packaging paper materials has also been carried out.

2. Theory and constitutive equations

2.1. Non-local theory: gradient enhanced approach

For a so-called local action approach one assumes that the mechanical state of the material at a given arbitrary point is independent of the state of the rest of the body, i.e. it is described only by the values of some fields at that point. Following such a point of view, in traditional models of damage mechanics, a damage variable enters the list of constitutive quantities (i.e. the description of the state).Its evolution is ruled by an ordinary differential equation. For models of this type, a problem of ill-posedness arises, namely balance equations loose their ellipticity at the transition from hardening to softening behavior. Strain localization phenomena occur in thin domains. Detailed discussions upon this topic are found in, among others, (cf. Pijaudier-Cabot and Bazant, 1987; Peerlings et al., 1996; Geers, 1997; Steinmann and Carol, 1998; de Borst et al., 1999; Kuhl and Ramm, 1999; Ganghoffer and de Borst, 2000; Comi, 2001; or Engelen et al., 2003). In the context of finite element solution techniques, one observes that the dissipation evaluated numerically vanishes as the mesh is refined.

Many investigators have tried to solve this problem and various models have been proposed. Successful attempts on the introduction of so-called non-local quantities into constitutive equations were proposed by Kröner (1967) and also by Eringen and Edelen (1972). Following their idea, the non-local counterpart $\bar{\tau}$ in a point x of a local state variable τ over an entire problem domain Ω with respect to a weight function ω is defined by (cf. Pijaudier-Cabot and Bazant, 1987)

$$\bar{\tau}(x) = \frac{1}{\Psi(x)} \int_{\Omega} \omega(\xi)\tau(x+\xi)\,\mathrm{d}\Omega(x). \tag{1}$$

The factor $\Psi^{-1}(x)$ with $\Psi(x)$ defined by

$$\Psi(x) = \int_{\Omega} \omega(\xi)\,\mathrm{d}\Omega(x), \tag{2}$$

scales $\bar{\tau}$ such that it equals τ for a homogenous state in the material. For simplicity the weight function ω is often (and also in this investigation) assumed to be homogenous and isotropic, i.e. it depends only on the distance $r = |x - \xi|$. However, the weight function ω may also be defined so as to include an anisotropic behavior.

The local state variable τ can be developed in a Taylor series around x and substituted into Eq. (1) resulting in a truncated explicit partial differential equation

$$\bar{\tau}(x) = \tau(x) + c\Delta\tau(x) \tag{3}$$

where the Laplacian operator is defined as $\Delta = \nabla^2 = \sum_i \frac{\partial^2}{\partial x_i^2}$.

Peerlings et al. (1996) approximated the explicit formulation in Eq. (3) with an implicit formulation resulting in an inhomogeneous elliptic equation

$$\bar{\tau}(x) - c\Delta\bar{\tau}(x) = \tau(x), \tag{4}$$

where terms of order four and higher have been neglected.

Since the non-local variable $\bar{\tau}$ depends implicitly on the corresponding local variable τ, Eq. (4) is referred to as the implicit gradient enhancement. For a study of various gradient enhanced formulations the interested reader is referred to Geers (1997), among others.

Throughout in the present study it is assumed that all non-local quantities (variables having a superposed bar, as in $\bar{\tau}$) admits at least Fréchet derivative. This is an inevitably necessity: if that would not be the case Eq. (4) could not make sense.

The gradient parameter c in Eq. (4) is given by $c = l^2/2$, where l is a characteristic length parameter that determines the volume that contributes significantly to the non-local state variable and must therefore be related to the scale of the micro-structure in the paper material. The introduction of a material characteristic length fixes the width of the zone in which localization occur, thus preventing localization into a vanishingly small region with zero energy dissipation. As in the case for the weight function ω, the gradient parameter c may also be defined anisotropic. However, for simplicity c is in this investigation assumed homogeneous and isotropic.

The solution of the implicit non-local state variable $\bar{\tau}$ requires additional boundary conditions. Commonly (cf. Lasry and Belytschko, 1988; or Mühlhaus and Aifantis, 1991) the natural Neumann type boundary condition of a vanishing gradient is used along the boundary Γ surrounding the entire problem domain Ω,

$$n\nabla\bar{\tau} = 0. \tag{5}$$

Here, n is the normal to the boundary Γ. It should be underlined that a physical interpretation of this boundary condition is not clear, cf. Peerlings et al. (1996) or Kuhl et al. (2000).

2.2. Continuum damage coupled to plasticity

A common concept in most continuum damage theories (cf. Cordebois and Sidoroff, 1982; Hansen and Schreyer, 1994; or Zhu and Cescotto, 1995) is the so-called elastic energy equivalence principle, postulating that "the elastic energy of a damaged material is the same form as that of an undamaged material except that the stress σ_{ij} (strain) is replaced by the effective stress $\hat{\sigma}_{ij}$ (effective strain)".

Introducing a forth order damage tensor M_{ijkl}, the relation between the stress tensor σ_{ij} in the damage space and the stress tensor $\hat{\sigma}_{ij}$ in the effective stress space can be written as,

$$\hat{\sigma}_{ij} = M_{ijkl}\sigma_{kl}. \tag{6}$$

Accordingly, the relation between the elastic strain tensor $\varepsilon^{\mathrm{e}}_{ij}$ and the effective elastic strain tensor $\hat{\varepsilon}^{\mathrm{e}}_{ij}$ is given by $\hat{\varepsilon}^{\mathrm{e}}_{ij} = M^{-1}_{ijkl}\varepsilon^{\mathrm{e}}_{kl}$.

There are several ways to define the tensor M_{ijkl}. The formulation used in this investigation, proposed by Chow and Wang (1987), offers a simplified analysis if the principal directions of orthotropic damage are assumed to be aligned with the principal axes of orthotropic plasticity. The inverse of M_{ijkl} is written on a 6×6 matrix format as

$$\mathbf{M}^{-1} = \begin{bmatrix} 1-D_1 & 0 & 0 & 0 & 0 & 0 \\ 0 & 1-D_2 & 0 & 0 & 0 & 0 \\ 0 & 0 & 1-D_3 & 0 & 0 & 0 \\ 0 & 0 & 0 & (1-D_1)^{1/2}(1-D_2)^{1/2} & 0 & 0 \\ 0 & 0 & 0 & 0 & (1-D_1)^{1/2}(1-D_3)^{1/2} & 0 \\ 0 & 0 & 0 & 0 & 0 & (1-D_2)^{1/2}(1-D_3)^{1/2} \end{bmatrix} \tag{7}$$

The damage in the material is represented by internal variables D_i, corresponding to a material degradation in each orthotropic principal direction i of the material, $0 \leqslant D_i \leqslant 1$, where $D_i = 0$ corresponds to a virgin element while $D_i = 1$ corresponds to a fully damaged element.

Since the main objective is to develop constitutive equations for a plastic-damaged material, attention is confined to a purely mechanical theory assuming isothermal processes. It is often assumed (see among others; Lemaitre, 1985; or Maugin, 1992) that the Helmholz free energy in the material can be divided into several independent parts. The free energy associated with plastic flow and the free energy associated with damage processes are in this investigation assumed independent of each other. An expression for the total Helmholz free energy density ψ can be written as

$$\psi = \psi^{\mathrm{e}}(\sigma_{ij}, D_i) + \psi^{\mathrm{p}}(\varepsilon^{\mathrm{p}}_{\mathrm{e}}) + \psi^{\mathrm{d}}(D_{\mathrm{e}}). \tag{8}$$

Here, ψ^{e} is the elastic energy, ψ^{p} is the free energy due to plastic hardening and ψ^{d} is the free energy due to damage hardening. $\varepsilon^{\mathrm{p}}_{\mathrm{e}}$ is an accumulated effective plastic strain and the variable D_{e} is an effective measure of damage.

The thermodynamic force Y_i conjugated to damage is often referred to as the "damage energy release rate" and is defined by

$$Y_i = -\frac{\partial \psi^{\mathrm{e}}}{\partial D_i}. \tag{9}$$

The force Y_i is regarded as the damaging driving-force and is understood to control the evolution of the damage. This definition is analogous to the definition of "fracture energy release rate" commonly used in theories of fracture mechanics.

Packaging paper materials are (as discussed in the introduction) considered as solids containing many long fibres connected in a network. At any point, those fibres apply non-local actions. It seems reasonable to assume that the mechanical state in one particular point in a fibre is dependent upon the mechanical states in the neighboring fibre network, or along the fibre itself. Hence, beside the numerical arguments discussed in Section 2.1, introduction of a non-local state variable is also supported by physical arguments in fibrous materials.

The idea of Kröner (1967) and Eringen and Edelen (1972) of introducing non-local quantities into a constitutive equation has been applied to continuum damage mechanics by several authors, among others Pijaudier-Cabot and Bazant (1987). For the damage model discussed in this investigation, a gradient enhanced damage energy release rate $\overline{Y_i}$ is introduced. Considering the local damage energy release rate Y_i as a state variable, Eq. (4) is restated as

$$\overline{Y}_i(x) - c\Delta\overline{Y}_i(x) = Y_i(x), \tag{10}$$

where $c = l^2/2$ and l is the internal length scale of the gradient enhancement.

The natural boundary condition of a vanishing gradient along all the entire boundary Γ of Ω is used,

$$n\nabla\overline{Y}_i = 0 \tag{11}$$

It is convenient to introduce the plastic hardening threshold H and the damage strengthening threshold R as the thermodynamic forces associated with ψ^{p} and ψ^{d}, respectively, i.e.

$$H = \frac{\mathrm{d}\psi^{\mathrm{p}}}{\mathrm{d}\varepsilon_{\mathrm{e}}^{\mathrm{p}}} \quad \text{and} \quad R = \frac{\mathrm{d}\psi^{\mathrm{d}}}{\mathrm{d}D_{\mathrm{e}}}. \tag{12}$$

A decomposition of the Helmholtz free energy according to Eq. (8) yields the well-known Clausius–Duhem inequality on a reduced form

$$\Phi = \sigma_{ij}\,\mathrm{d}\varepsilon_{ij}^{\mathrm{p}} - H\,\mathrm{d}\varepsilon_{\mathrm{e}}^{\mathrm{p}} - \overline{Y}_i\,\mathrm{d}D_i - R\,\mathrm{d}D_{\mathrm{e}} \geqslant 0 \tag{13}$$

where Φ is the mechanical dissipation.

A common way of ensuring the fulfillment of the Clausius–Duhem inequality $\Phi \geqslant 0$ consists of postulating the existence of convex, continuous and scalar valued potential functions ϕ dependent on all the thermodynamical forces with the internal state variables appearing as parameters, cf. Voyiadjis and Kattan (1992). Within the assumption of independence of energy dissipations Φ is divided into two parts $\Phi = \Phi^{\mathrm{p}} + \Phi^{\mathrm{d}}$, where

$$\Phi^{\mathrm{p}} = \sigma_{ij}\mathrm{d}\varepsilon_{ij}^{\mathrm{p}} - H\mathrm{d}\varepsilon_{\mathrm{e}}^{\mathrm{p}} - \lambda^{\mathrm{p}}\phi^{\mathrm{p}} \geqslant 0, \tag{14}$$

and

$$\Phi^{\mathrm{d}} = -\overline{Y}_i\mathrm{d}D_i - R\,\mathrm{d}D_{\mathrm{e}} - \lambda^{\mathrm{d}}\phi^{\mathrm{d}} \geqslant 0. \tag{15}$$

Here, the plastic and damage multipliers $\lambda^{\mathrm{p}}, \lambda^{\mathrm{d}} \geqslant 0$ are introduced and they are determined by the consistency requirements $\mathrm{d}\phi^{\mathrm{p}} = \mathrm{d}\phi^{\mathrm{d}} = 0$ together with the loading/unloading conditions $\phi^{\mathrm{p}} = \phi^{\mathrm{d}} = 0$. As indicated by Eqs. (14) and (15) represents ϕ^{p} the plastic yield criterion and ϕ^{d} represents the damage criterion.

As the reduced Clausius–Duhem inequality fulfill $\Phi \geqslant 0$, meaning that the production of internal entropy always is positive, the chosen model is admissible from a thermodynamic point of view. Hence, the model is thermodynamically consistent.

2.3. Anisotropic plasticity

The plastic processes are commonly assumed connected to the effective stress space since the effective stress $\hat{\sigma}_{ij}$ is referred to a surface in the material that really transmits the internal forces, (see amid others Simo and Ju, 1987; Ju, 1989; Lemaitre and Chaboche, 1990; or Contrafatto and Cuomo, 2002).

Assuming the material axes of orthotropy coincides with the principal axes, Hill's yield criterion (Hill, 1950) offers a convenient way to introduce anisotropic plasticity. The yield surface is in this case given by the expression

$$\phi^{\mathrm{p}} = \hat{\sigma}_{\mathrm{e}} - H \leqslant 0, \tag{16}$$

where $\hat{\sigma}_{\mathrm{e}}$ is the anisotropic equivalent stress defined in analogy with the J_2-flow theory of plasticity,

$$\hat{\sigma}_{\mathrm{e}} = \sigma_{\mathrm{y0}}(\hat{s}_{ij}P_{ijkl}\hat{s}_{kl})^{1/2}. \tag{17}$$

The plastic threshold $H(\hat{\varepsilon}^{\mathrm{p}}_{\mathrm{e}})$ is as the maximum value that the anisotropic equivalent stress $\hat{\sigma}_{\mathrm{e}}$ has reached during the deformation history (with the initial value σ_{y0}), thus representing an isotropic strain hardening plasticity behavior of the material. The isotropic hardening represents a global expansion in the size of the yield surface with no change in shape. The threshold H can often be determined from experiments.

The deviatoric effective stress tensor is given by $\hat{s}_{ij} = \hat{\sigma}_{ij} - \delta_{ij}\hat{\sigma}_{kk}/3$. Here repeated index assumes summation and δ_{ij} is the Kronecker delta. The positive definite tensor P_{ijkl} for orthotropic materials can be represented by a 6×6 matrix $\mathbf{P}$,

$$\mathbf{P} = \begin{bmatrix} p_{12}+p_{13} & -p_{12} & -p_{13} & 0 & 0 & 0 \\ -p_{12} & p_{12}+p_{23} & -p_{23} & 0 & 0 & 0 \\ -p_{13} & -p_{23} & p_{23}+p_{13} & 0 & 0 & 0 \\ 0 & 0 & 0 & p_4 & 0 & 0 \\ 0 & 0 & 0 & 0 & p_5 & 0 \\ 0 & 0 & 0 & 0 & 0 & p_6 \end{bmatrix}, \tag{18}$$

where p_{12}, p_{13}, p_{23}, p_4, p_5, p_6 are parameters characterizing the current state of plastic anisotropy. In the particular case when $3p_{12} = 3p_{13} = 3p_{23} = p_4 = p_5 = p_6 = 3/(2\sigma^2_{\mathrm{y0}})$ this yield criterion is reduced to the J_2 -theory of plasticity.

The outward normal of the yield surface is given by

$$\frac{\partial\phi^{\mathrm{p}}}{\partial\hat{\sigma}_{ij}} = \frac{\sigma^2_{\mathrm{y0}}}{\hat{\sigma}_{\mathrm{e}}}P_{ijkl}\hat{s}_{kl}. \tag{19}$$

Normality of the plastic strain increment requires that

$$\mathrm{d}\hat{\varepsilon}^{\mathrm{p}}_{ij} = \lambda^{\mathrm{p}}\frac{\partial\phi^{\mathrm{p}}}{\partial\hat{\sigma}_{ij}}. \tag{20}$$

As the hardening is assumed being isotropic, λ^{p} may be determined from a uniaxial tensile test with the test specimen oriented in the material directions. Thus, λ^{p} is assigned different values depending on the direction of loading. For a uniaxial tensile test in the x_1-direction, consider the stress state $\hat{\sigma}_{11} = \hat{\sigma} = \hat{\sigma}_{\mathrm{e}}$, all other $\hat{\sigma}_{ij} = 0$, and $\hat{\varepsilon}_{11} = \hat{\varepsilon}^{\mathrm{e}}_{11} + \hat{\varepsilon}^{\mathrm{p}}_{11} = \hat{\varepsilon}$. One finds

$$\lambda^{\mathrm{p}} = \frac{3\sigma_{\mathrm{y}0}}{2\hat{\sigma}E}(E/E_t - 1)\,\mathrm{d}\hat{\sigma}, \tag{21}$$

where E is the elastic modulus in the loading direction of the material and $E_t = \mathrm{d}\hat{\sigma}/\mathrm{d}\hat{\varepsilon}$ is the tangent modulus for the uniaxial tensile test at the stress level $\hat{\sigma} = \hat{\sigma}_{\mathrm{e}} > \sigma_{\mathrm{y}0}$.

Since $\mathrm{d}\hat{\sigma}_{\mathrm{e}} = (\sigma_{\mathrm{y}0}^2/\hat{\sigma}_{\mathrm{e}})\hat{s}_{ij}P_{ijkl}\mathrm{d}\hat{\sigma}_{kl}$, the expression for the plastic strain increment $\mathrm{d}\hat{\varepsilon}_{ij}^{\mathrm{p}}$ in a general form can be written as

$$\mathrm{d}\hat{\varepsilon}_{ij}^{\mathrm{p}} = \gamma\frac{3\sigma_{\mathrm{y}0}^4}{2\hat{\sigma}_{\mathrm{e}}^2E}(E/E_t - 1)P_{ijkl}\hat{s}_{kl}\hat{s}_{mn}P_{mnop}\,\mathrm{d}\hat{\sigma}_{op}, \tag{22}$$

where

$$\gamma = \begin{cases} 1 & \text{for } \hat{\sigma}_{\mathrm{e}} = H \quad \text{and} \quad \mathrm{d}\hat{\sigma}_{\mathrm{e}} \geqslant 0 \\ 0 & \text{else} \end{cases} \tag{23}$$

Assuming a modified uniaxial Ramberg–Osgood relation $\hat{\varepsilon} = \hat{\sigma}/E + \sigma_{\mathrm{y}0}(\hat{\sigma}/\sigma_{\mathrm{y}0})^n$ the relation E/E_t may be written as

$$E/E_t = (\hat{\sigma}_{\mathrm{e}}/\sigma_{\mathrm{y}0})^{n-1}, \tag{24}$$

where $n \geqslant 1$ denote the hardening exponent in the test direction.

Generally, if the paper material exhibits different hardening behavior in different material directions and the body is subjected to a multiaxial loading situation, the model needs to be extended with a model for anisotropic hardening in which case multiaxial material parameters have to be invoked, cf. Xia et al. (2002).

The elastic strain increment in the effective stress space is given by $\mathrm{d}\hat{\varepsilon}_{ij}^{\mathrm{e}} = C_{ijkl}^{-1}\mathrm{d}\hat{\sigma}_{kl}$. The inverse of the orthotropic stiffness tensor C_{ijkl} is on a 6×6 matrix format written as

$$\mathbf{C}^{-1} = \begin{bmatrix} E_1^{-1} & -v_{12}E_1^{-1} & -v_{13}E_1^{-1} & 0 & 0 & 0 \\ -v_{21}E_2^{-1} & E_2^{-1} & -v_{23}E_2^{-1} & 0 & 0 & 0 \\ -v_{31}E_3^{-1} & -v_{32}E_3^{-1} & E_3^{-1} & 0 & 0 & 0 \\ 0 & 0 & 0 & (2G_{12})^{-1} & 0 & 0 \\ 0 & 0 & 0 & 0 & (2G_{13})^{-1} & 0 \\ 0 & 0 & 0 & 0 & 0 & (2G_{23})^{-1} \end{bmatrix} \tag{25}$$

where E_i represents the in-plane elastic modulus, v_{ij} are the in-plane Poissonś ratios and G_{ij} denotes the in-plane shear modulus.

The total strain increment in the effective space is given as the sum of the elastic and plastic strain increments, $\mathrm{d}\hat{\varepsilon}_{ij} = \mathrm{d}\hat{\varepsilon}_{ij}^{\mathrm{e}} + \mathrm{d}\hat{\varepsilon}_{ij}^{\mathrm{p}}$. Using the elastic stress–strain relationship, written in the form $\mathrm{d}\hat{\sigma}_{ij} = C_{ijkl}(\mathrm{d}\hat{\varepsilon}_{kl} - \mathrm{d}\hat{\varepsilon}_{kl}^{\mathrm{p}})$, yields for plastic yielding

$$\mathrm{d}\hat{\sigma}_{ij} = C_{ijkl}\mathrm{d}\hat{\varepsilon}_{kl} - \theta C_{ijkl}P_{klmn}\hat{s}_{mn}\hat{s}_{op}P_{opqr}\mathrm{d}\hat{\sigma}_{qr}, \tag{26}$$

where

$$\theta = \frac{3\sigma_{\mathrm{y}0}^4}{2\hat{\sigma}_{\mathrm{e}}^2E}(E/E_t - 1). \tag{27}$$

Multiplication of this expression by $\hat{s}_{ij}P_{ijkl}$ leads to an equation from which the inner product $\hat{s}_{ij}P_{ijkl}\mathrm{d}\hat{\sigma}_{kl}$ is determined as a function of the effective strain increment $\mathrm{d}\hat{\varepsilon}_{mn}$

$$\hat{s}_{ij}P_{ijkl}\mathrm{d}\hat{\sigma}_{kl} = \frac{\hat{s}_{ij}P_{ijkl}C_{klmn}}{1 + \theta\hat{s}_{op}P_{opqr}C_{qrst}P_{stuv}\hat{s}_{uv}}\mathrm{d}\hat{\varepsilon}_{mn}. \tag{28}$$

Substituting Eq. (28) into Eq. (26) gives the well-known elastic–plastic incremental stress–strain relation

$$\mathrm{d}\hat{\sigma}_{ij} = C_{ijst}\mathrm{d}\hat{\varepsilon}_{st} - \mu C_{ijkl}P_{klmn}\hat{s}_{mn}\hat{s}_{op}P_{opqr}C_{qrst}\mathrm{d}\hat{\varepsilon}_{st} = C_{ijst}^{\mathrm{ep}}\mathrm{d}\hat{\varepsilon}_{st}, \tag{29}$$

where C^{ep}_{ijkl} is the incremental elastic–plastic stiffness tensor in the effective space and

$$\mu = \begin{cases} \dfrac{\theta}{1+\theta\hat{s}_{ij}P_{ijkl}C_{klmn}P_{mnop}\hat{s}_{op}} & \text{for } \hat{\sigma}_{\mathrm{e}} = H \quad \text{and} \quad \mathrm{d}\hat{\sigma}_{\mathrm{e}} \geqslant 0, \\ 0 & \text{else.} \end{cases} \tag{30}$$

2.4. Anisotropic damage evolution

Assuming that the material axes of orthotropy coincides with the principal axes, a damage criterion in the form of a quadratic homogeneous convex function of the gradient enhanced damage release rate $\overline{Y}_i$ offers a convenient way to model orthotropic damage evolution,

$$\phi^{\mathrm{d}} = \overline{Y}_{\mathrm{e}} - R \leqslant 0. \tag{31}$$

One may note the similarity between Eq. (31) and the corresponding criterion for plastic flow, Eq. (16). The equivalent non-local damage energy release rate $\overline{Y}_{\mathrm{e}}$ is defined as

$$\overline{Y}_{\mathrm{e}} = (\overline{Y}_i J_{ij} \overline{Y}_j/2)^{1/2}, \tag{32}$$

where J_{ij} is a second order positive damage characteristic tensor that will be discussed later.

The threshold $R(D_{\mathrm{e}})$ is interpreted as the maximum value that $\overline{Y}_{\mathrm{e}}$ has reached during the deformation history (with the initial value Y_0), representing a damaging hardening material.

The criterion in Eq. (31) was initially introduced on local form by Cordebois and Sidoroff (1982) and further discussed in Chow and Wang (1987), Hansen and Schreyer (1994) or Zhu and Cescotto (1995) among others. It should be underlined that the only difference between the present criterion and the criterion introduced by Cordebois and Sidoroff (1982) is the presence of the non-local damage energy release rate $\overline{Y}_i$, which is the non-local counterpart of the local damage energy release rate $Y_i = -\hat{\sigma}_{mn}C^{-1}_{mnkl}\partial\hat{\sigma}_{kl}/\partial D_i$ (Eq. (11)).

Using an associated law, normality of the damage increments requires that

$$\mathrm{d}D_i = -\lambda^{\mathrm{d}}\frac{\partial\phi^{\mathrm{d}}}{\partial\overline{Y}_i} \tag{33}$$

and

$$\mathrm{d}D_{\mathrm{e}} = -\lambda^{\mathrm{d}}\frac{\partial\phi^{\mathrm{d}}}{\partial R}. \tag{34}$$

The multiplier λ^{d} can be determined from experiments by applying the consistency requirement $\mathrm{d}\phi^{\mathrm{d}} = 0$ and the loading/unloading condition $\phi^{\mathrm{d}} = 0$.

The damage characteristic tensor J_{ij} has been extensively discussed in the literature and many formulations have been suggested. A comprehensive review of the most widely used expressions is presented in Voyiadjis and Park (1997). However, a symmetric damage characteristic tensor J_{ij} of second order, introduced by Zhu and Cescotto (1995), is believed to be applicable for the circumstances discussed here. The characteristic tensor J_{ij} is on 3×3 matrix format written as

$$\mathbf{J} = 2\begin{bmatrix} g_1 & (g_1g_2)^{1/2} & (g_1g_3)^{1/2} \\ (g_1g_2)^{1/2} & g_2 & (g_2g_3)^{1/2} \\ (g_1g_3)^{1/2} & (g_2g_3)^{1/2} & g_3 \end{bmatrix}. \tag{35}$$

Here, g_i depends on the damage evolution history in the material in direction i.

For an equivalent damage formulation, the total damage work W performed at time t should be the same as the equivalent damage work performed at time t, i.e.

$$W = \int_0^{D_i(t)} \overline{Y}_i \,\mathrm{d}D_i = \int_0^{D_\mathrm{e}(t)} \overline{Y}_\mathrm{e} \,\mathrm{d}D_\mathrm{e}. \tag{36}$$

Then, according to Zhu and Cescotto (1995),

$$g_i = (\overline{Y}_\mathrm{e}/\overline{Y}_i)^2. \tag{37}$$

Two different damage evolution laws is utilized in the present investigation:

(i) A linear damage evolution law on the form (cf. Zhu and Cescotto, 1995),

$$\frac{\mathrm{d}D_\mathrm{e}}{\mathrm{d}\overline{Y}_\mathrm{e}} = k_\mathrm{e}. \tag{38}$$

(ii) An exponential damage evolution law on the form (cf. Geers, 1997),

$$\frac{\mathrm{d}D_\mathrm{e}}{\mathrm{d}\overline{Y}_\mathrm{e}} = k_\mathrm{e}(1 - D_\mathrm{e}). \tag{39}$$

Here, k_e is the equivalent damage hardening value.

3. Numerical implementation

The above-described constitutive relations have been used to analyze the mechanical behavior of paper materials. The governing equations have been solved using the finite element method. The finite element computations have been performed with the mathematical program Matlab (2002). A state of plane stress is considered throughout in the computations.

The constitutive laws described in the preceding sections have been implemented for a two-dimensional solid material element. Four-node isoparametric elements, with two degrees of freedom, translation in the x_1- and x_2-directions, have been utilized.

Pertinent material property data for the various materials, obtained in tensile tests, have been used in the simulations.

An iterative technique has been employed to solve the discretized equilibrium equations for each load step. The result obtained after each iteration then correspond to estimates of the incremental displacements from which the currents stress and strain states can be computed at the integration points of each finite element, as well as estimates of the non-local damage energy release rate. The deformations are assumed to remain small, so all derivatives and integrals are evaluated with respect to the initial topology of the considered body.

A modified Newton–Raphson iteration scheme for the solution of non-linear finite element equations has been employed (cf. Bathe, 1982). The governing finite element equation is

$$\mathbf{KA} = \mathbf{R} - \mathbf{F}, \tag{40}$$

where **K** is the global stiffness matrix, **A** is the global vector consisting of nodal displacement variables and non-local damage energy release rates, **R** is the vector of externally applied nodal point loads and **F** represents the vector of nodal point forces equivalent to the element stresses. It should be noted that at each node the displacement field, as well as the non-local damage energy release rates, are represented by vectorial fields.

The finite element implementations follows mainly the ones discussed in Peerlings et al. (1996) and Geers (1997) for the enhanced gradient model. For easy-to-use manuals of the implementations the reader is advised to Peerlings et al. (2000) or Geers (1997).

The relation in Eq. (40) is employed to calculate increments in the displacements and non-local damage energy release rates, which then is used to evaluate approximations corresponding to time (or load step) $t+\Delta t$,

$$ {}^{t+\Delta t}\mathbf{K}^{(i-1)}\Delta\mathbf{A}^{(i)} = {}^{t+\Delta t}\mathbf{R} - {}^{t+\Delta t}\mathbf{F}^{(i-1)}, \tag{41} $$

where

$$ {}^{t+\Delta t}\mathbf{A}^{(i)} = {}^{t+\Delta t}\mathbf{A}^{(i-1)} + \Delta\mathbf{A}^{(i)}. \tag{42} $$

The superscript (i) denote the iteration number value and the vector $\Delta\mathbf{A}^{(i)}$ represents the increment in the solution variable at iteration (i). This results in a system of linear algebraic equations, which are solved at each equilibrium iteration. The iterations are continued until appropriate convergence criteria are satisfied (cf. Bathe, 1982; or Cook et al., 1989).

As a consequence of the assumption that the relation between the stresses in the damage space and the effective space is given by $\sigma_{ij} = M^{-1}_{ijkl}\hat{\sigma}_{kl}$, a linearized expression for the stress increments at load step $t+\Delta t$ of the stress tensor σ_{ij} is obtained as

$$ {}^{(t+\Delta t)}\Delta\sigma_{ij} = {}^{(t)}M^{-1}_{ijkl}\,{}^{(t+\Delta t)}\Delta\hat{\sigma}_{kl} + {}^{(t)}\Delta M^{-1}_{ijkl}\,{}^{(t)}\hat{\sigma}_{kl}. \tag{43} $$

4. Experiments

Two types of commercial packaging paper were investigated in terms of load–elongation curves. The objective was to determine the applicability of the model derived. Of particular interest is transferability, i.e. that one set of model parameters can describe the mechanical response of significantly different geometries.

4.1. Test set-up and test procedure

An MTS Universal Tensile Testing Machine, equipped with a pair of wide clamps, was used to measure the load–elongation response, Fig. 3. Locking pins at the center of the front jaws keep the clamps in an open position during mounting of the specimen. After positioning of the specimen the upper and lower clamp are closed and the pressure is applied by tightening four equally spaced quick-acting locking nuts along the front of each clamp. The largest sample that can be accommodated is 420 mm wide.

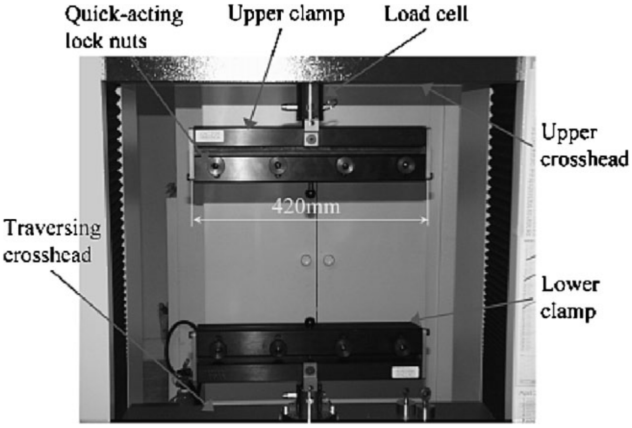

Fig. 3. Universal tensile tester equipped with a pair of wide clamps.

The load frame is equipped with a 2 kN load cell. Specimens were tested by traversing the lower cross-head down to place the sample under increasing load at a constant cross-head speed at nominal strain rate of 20%/min. The samples were pre-loaded up to 1 N, before recording of data started.

During testing, both displacement and load was monitored and recorded. The load was measured by the load cell and the elongation by recording the cross-head movement. A computer was used to control the load frame and also to record data during the testing. All tests were run to failure.

Mechanical testing of paper must be carried out under humidity and temperature control, in order to obtain reproducible results since paper is strongly influenced by moisture. The climate used was 23 °C and 50% RH and is in accordance with ISO 187. The samples were conditioned for at least 48 h in this climate prior to testing.

4.2. Materials and manufacturing of the specimen

Two types of packaging paper materials were examined. One denoted Kraftliner, i.e. paper mainly made of unbleached sulfate pulp, and one denoted Testliner consisting entirely of recycled fibres. Some important properties of the material are listed in Table 1.

Standard methods were used to test structural properties. The standards used are ISO 534 for thickness and ISO 536 for basis weight.

Four different specimen geometries have been used: a rectangular geometry having a width of 15 mm and a gauge length of 100 mm, a specimen with a notch radius of 5 mm, width 50 mm and a gauge length of 10 mm, a specimen with a semi-circular notch of radius 5 mm having an outer width of 50 mm and a gauge length of 40 mm, and a specimen with a semi-circular notch of radius 31.75 mm having an outer width of 133 mm and a gauge length of 126 mm. The specimens, illustrated in Fig. 4, are from now on denoted specimen I–IV, respectively.

Table 1
Some material properties

	Thickness	Basis weight	Average fibre length	Recycle fibre content	Virgin fibre content
Kraftliner	0.164 mm	125 kg/m^2	1.25 mm	30%	70%
Testliner	0.185 mm	127 kg/m^2	1.06 mm	100%	0%

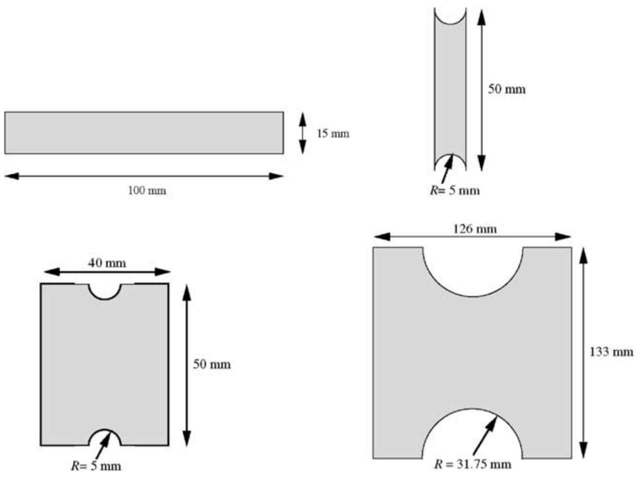

Fig. 4. Considered specimen (I–IV) geometries.

The notched samples were used in order to control the localization of failure. Two different sizes of notched specimens (III and IV) have been used in order to evaluate the transferability between different geometries.

The specimens denoted I and IV were fabricated using a razor knife, whereas specimens II and III where manufactured using a punch. Normally five specimens of each type were tested in each in-plane material direction, i.e. both in MD and CD.

5. Limitations and general and additional assumptions

As discussed in the experiment section, the Kraftliner paper specimens are about 0.164 mm thick, whereas the Testliner paper specimens are about 0.185 mm thick. Hence, as the thickness of the specimens is negligible in comparison to the width and the lengths of the specimens, a state of plane stress is considered throughout the computations.

For simplicity, the material is assumed to have the same behavior in Z as in CD, which significantly reduces the complexity when determining the material parameters.

It is possible to identify at least two damage processes for paper materials, e.g. fibre/fibre bond failure and fibre breakage. In this study it is assumed that there is one dominating damage process during tensile loading of a paper structure, even though there is nothing assumed about the nature of it.

If the material exhibits different hardening behavior in different material directions and the body is subjected to a multiaxial loading situation, the model needs to be extended with a model for anisotropic hardening whereupon new material parameters have to be invoked.

6. The model

6.1. Calibration of the constitutive model and determination of material parameters

The calibration procedure of the constitutive model is briefly explained here. Because the model is two-dimensional, only in-plane material constants needs to be determined. The model parameters were determined using load–elongation curves obtained for the two different specimens I and II (see Fig. 4).

The materials were tested in both in-plane material directions, i.e. both MD and CD.

The specimen denoted specimen I is a slender geometry resulting in an approximately uniaxial stress state when loaded in tension. This type is used for determining the elastic constants of the material and to estimate the initial yield stress and hardening parameters of the plasticity model. Values of the Poisson's ratios have been taken from literature (Baum et al., 1981) together with the demands of symmetry imposed on the stiffness tensor C_{ijkl}, i.e. $\nu_{21}/E_1 = \nu_{12}/E_2$. The in-plane shear modulus G_{12} is assigned the value

$$G_{12} = \frac{(E_1 E_2)^{1/2}}{2[1 + (\nu_{12}\nu_{21})^{1/2}]}, \tag{44}$$

following the results reported by Szilard (1974). The in-plane yield shear stress is in all computations assigned the value $3^{-1/2}\sigma_{y0}$, cf. Hill (1950).

The damage hardening parameters were obtained from the descending part of load–elongation curves, obtained in tension tests using specimen II. This part of the curve can only be obtained if the damage process is stable (or semi-stable). In a stable damage process, the stress continuously decreases as the displacement is increased up to total separation of two fracture surfaces. For packaging paper materials, this behavior can only be obtained at a relatively short gauge length, cf. Tryding (1996). If the gauge length is too long, lots of elastic energy will be stored in the specimen prior to peak load and released in an unstable manner at a post peak-load elongation. Specimens denoted specimen II has been used in order to measure the load–elongation response in the descending regime. These specimens proved to be capable of generating stable descending curves for the considered materials.

A numerical procedure has been implemented in order to fit the equivalent damage hardening parameters k_e to the measured load–elongation curves.

6.2. Boundary conditions

The symmetry of the specimens and the loading conditions allow us to model only a quarter of the specimen geometries. The dimensions for a portion of the test specimens I and II, in the x_1- and x_2-directions, are as shown in Fig. 5.

The natural boundary condition of a vanishing gradient is adopted on all edges,

$$n\nabla\overline{Y}_i = 0. \tag{45}$$

In addition to the boundary condition in Eq. (45), the edges A, B, and C are subjected to the boundary conditions

$$\begin{cases} \mathrm{A}: & u = \sigma_{12} = 0, \\ \mathrm{B}: & v = \sigma_{12} = 0, \\ \mathrm{C}: & v = 0 \quad \text{and} \quad u = U. \end{cases} \tag{46}$$

The displacements u and v are in the x_1- and x_2-directions, respectively. The normal traction is zero only along edge D, which is the only traction free surface in the model.

At edge C the nodes are constrained to a straight vertical line between the two corner nodes, which are given the prescribed displacement U. All the nodes along edge C are also constrained to have zero displacement in the x_2-direction, i.e. $v = 0$ along C. To preserve vertical compatibility, the nodes along edge A are constrained to have zero displacement in the x_1-direction, i.e. $u = 0$ along A.

In addition, the nodes along edge A are free to move in the x_2-direction.

As a result of the imposed boundary conditions on specimen I, the stress field is nearly homogeneous leading to a simultaneous initiation of damage growth throughout the specimen. To avoid this, an initial imperfection is introduced in the specimen in a small region in the center of the specimen in order to trig and localize damage initiation. The region containing an initial imperfection, or damage, of $D_1 = D_2 = 0.02$

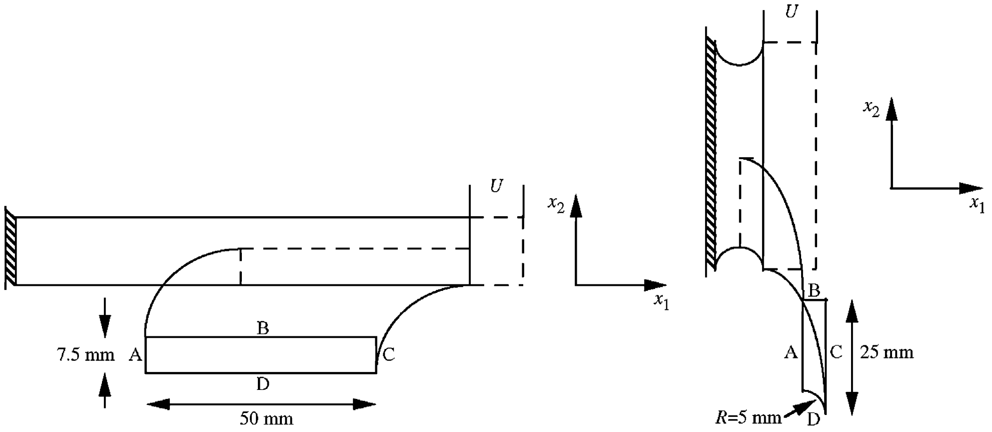

Fig. 5. Schematic representations of portions of the modeled test specimens I and II.

occupies the region $49.0 \leqslant x_1 \leqslant 50.0$ mm and $6.43 \leqslant x_2 \leqslant 7.5$ mm, corresponding to a fraction of 0.3% of the total specimen volume.

6.3. The characteristic length l

Generally, mesh refinement leads to localized deformation in a region of decreasing volume if damage is invoked in the constitutive equations. When the gradient enhanced approach is adapted (i.e. $l > 0$) this problem is avoided and the density of the finite element mesh is not crucial, cf. Geers (1997) or Kuhl and Ramm (1999). Hence, the constitutive model requires a material parameter l of dimension length (i.e. a characteristic length that controls the extent of the zone in which localization occur). However, there exist no obvious physical interpretation of this parameter. It is desirable to find an inherent property of the material that can be related to this parameter.

Fig. 6 shows a SEM picture of a damaged region in a Testliner specimen III loaded in CD until failure. An intuitive choice is to relate the gradient length l to the mean fibre length in the material. This assumption has to some extent support from previous investigations. Niskanen et al. (2001) showed in an experimental investigation, that the width of the damage band, developing when a paper specimen is loaded in tension until failure, is governed by the fibre length. Their experiments were conducted on so-called handsheets, i.e. in-plane isotropic sheets manufactured in a laboratory environment.

Niskanen et al. concluded that the damage width is linearly proportional to the mean fibre length. However, the authors underlined that the damage width also can be affected by other factors such as the mechanical properties of the fibres and manufacturing conditions.

As the fibre length average (see Table 1) for Kraftliner and for Testliner both are on the same order of magnitude ($\approx$1 mm) one expects, according to the results reported by Niskanen et al. (2001), that the characteristic length l is almost the same for Kraftliner and for Testliner.

During the course of this investigation, it has been found that the value $l = 2$ mm generates reasonable correspondence between the experiments and the numerical analysis for both Kraftliner and Testliner. This result indicates that the characteristic length parameter in a gradient enhanced approach can be related to the average fibre length in the paper material as the value of l equals approximate $l \approx 2l_\mathrm{f}$ where l_f is the average fibre length.

6.4. Results of parameter estimation

The experiments have been analyzed in a FE model in order to verify the measured material parameters. The finite element meshes used for the material parameter verification computations are shown in Fig. 7.

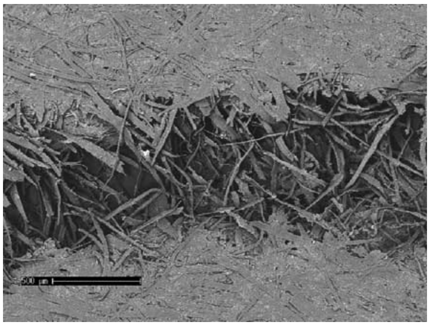

Fig. 6. Damaged region in a Testliner specimen III loaded in CD. The magnification of the sample is 80× and the length indicator in the black area corresponds to 0.5 mm.

Fig. 8 displays load–elongation curves obtained from the uniaxial tensile test using specimen I made of the two paper materials and loaded in MD and CD, respectively, together with numerical results. The

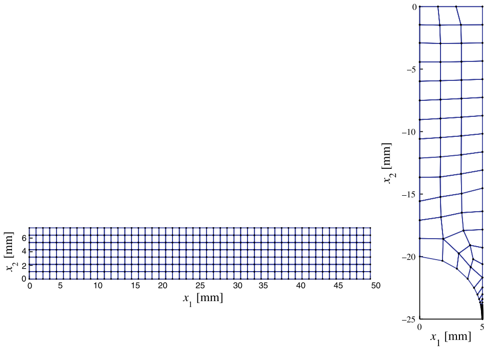

Fig. 7. Finite element meshes used for the material parameter verification. The meshes consists of 350 elements (specimen I) and 92 elements (specimen II).

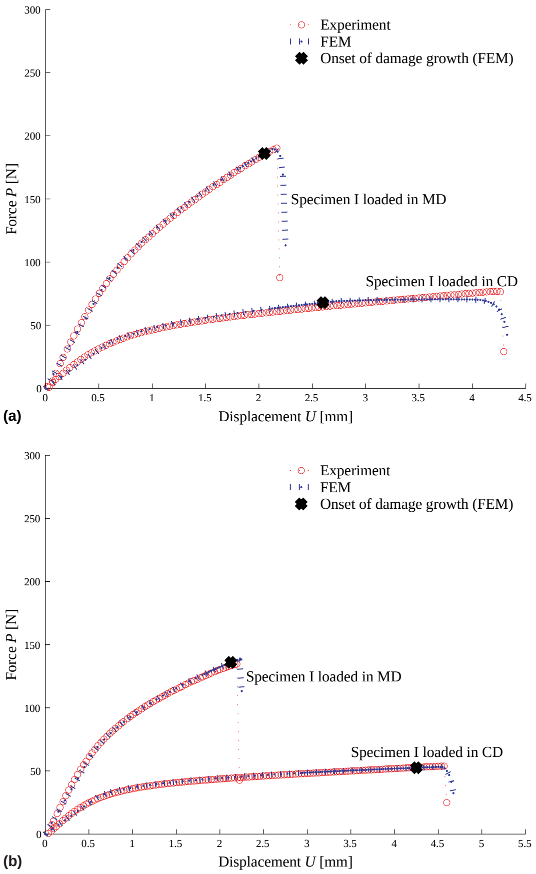

Fig. 8. Load–elongation curves obtained from the uniaxial tensile tests using specimen I made of Kraftliner (a) and Testliner (b). Computed results are also displayed.

exponential damage evolution law in Eq. (39) has been utilized. The computed onsets of damage growth are also indicated. As Fig. 8 illustrates, excellent agreement prevails between the measured load–elongation curves and the numerical results.

The experimentally obtained descending curves using specimen II are compared to numerical results from FE computations (Fig. 9) when three different values of the equivalent hardening parameter k_e have been employed ($k_\mathrm{e} = 1, 5, 20$ $(\mathrm{MPa\,mm})^{-1}$ for Kraftliner and $k_\mathrm{e} = 10, 20, 30$ $(\mathrm{MPa\,mm})^{-1}$ for Testliner).

A conclusion one may draw from Fig. 9 is that an equivalent damage hardening value $k_\mathrm{e} = 5$ $(\mathrm{MPa\,mm})^{-1}$ for Kraftliner and $k_\mathrm{e} = 20$ $(\mathrm{MPa\,mm})^{-1}$ for Testliner describes the damage hardening in the specimen reasonable well in both MD and CD. For simplicity, the damage hardening is assumed to be the same in the principal directions of the material (compare with isotropic strain hardening), i.e. $k_1 = k_2 = k_\mathrm{e}$.

The material parameters determined from tensile experiments using specimens I + II and by numerical studies are summarized in Tables 2 and 3 (MD is along the x_1-direction).

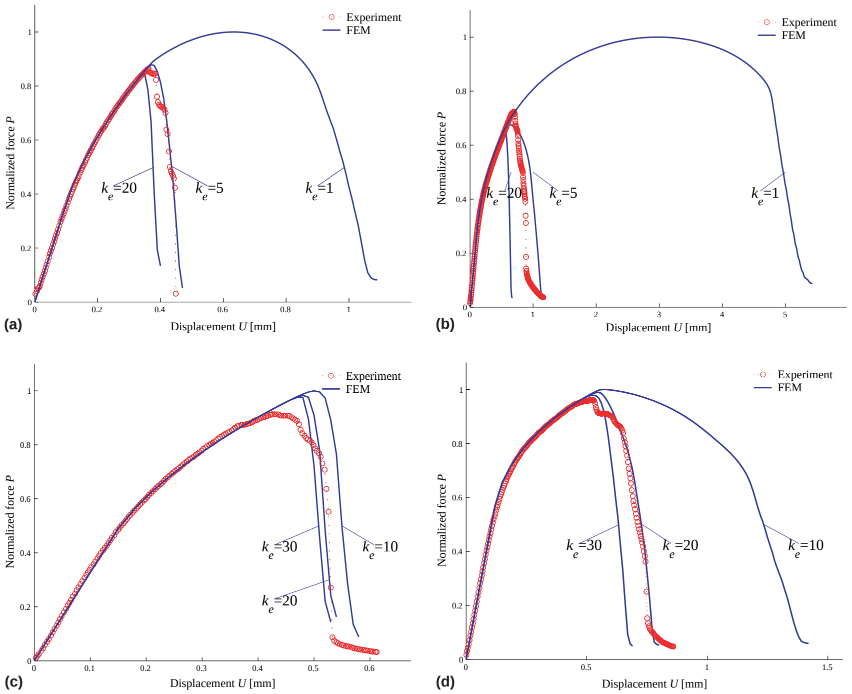

Fig. 9. Numerical results obtained with different values of the hardening parameter k_e compared to experimentally obtained descending curves. Kraftliner loaded in MD (a) and CD (b). Testliner loaded in MD (c) and CD (d).

Table 2
Material parameters obtained from tensile experiments using specimen I

	Kraftliner	Testliner
E_1	1280 MPa mm	900 MPa mm
E_2	470 MPa mm	400 MPa mm
ν_{12}	0.46	0.46
$\sigma^1_{\mathrm{y}0}$	4.5 MPa mm	3.6 MPa mm
$\sigma^2_{\mathrm{y}0}$	2.0 MPa mm	1.8 MPa mm
n_1	1.8	2.2
n_2	3.0	4.8

Table 3
Material parameters determined by numerical studies using specimen I + II. The initial threshold parameters for damage growth in the x_1- and x_2-direction are denoted Y_{10} and Y_{20} respectively

	Kraftliner	Testliner
Y_{10}	0.16 MPa mm	0.11 MPa mm
Y_{20}	0.05 MPa mm	0.04 MPa mm
k_e	5 $(\text{MPa mm})^{-1}$	20 $(\text{MPa mm})^{-1}$
l	2 mm	2 mm

6.5. The damage evolution law

Two damage evolution laws implemented have been compared; the linear evolution law (Eq. (38)) and the exponential evolution law (Eq. (39)).

The total evolution of the equivalent damage D_e at time t according to the two laws is slightly different. For the linear evolution law one have (Y_0 is the initial damage threshold value)

$$D_e(t) = k_e[\overline{Y}_e(t) - Y_0], \tag{47}$$

and for the exponential evolution law one have

$$D_e(t) = 1 - e^{-k_e(\overline{Y}_e(t) - Y_0)}. \tag{48}$$

The last mentioned damage law is naturally bounded meaning that it allows continuous description of fully damaged material as the resulting damage is close to (but remain smaller than) 1. Hence, the exponential damage evolution law is particular convenient from a numerical point of view since it allows the stiffness matrix of the structure to remain regular.

This feature can also been seen in Fig. 10 where normalized load–elongation curves for a specimen II loaded in CD and made of Testliner is displayed. When using the exponential evolution law, the computed load–elongation path is smooth and follows the descending part down to total breakage of the specimen. In contrast, when the linear damage law is used the stiffness matrix becomes irregular at an earlier load step, leading to an earlier (modeled) breakage of the specimen.

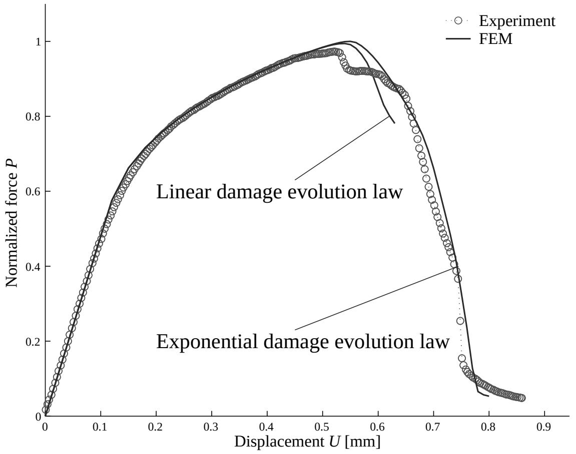

Fig. 10. Normalized numerical results obtained utilizing the two damage evolution laws, Eqs. (38) and (39), compared to an experimentally load–elongation curve. The Testliner specimen II was loaded uniaxially in CD.

It can be mentioned here that an ongoing laboratory investigation by the authors (Gradin and Isaksson, submitted) reveals that the exponential damage evolution law utilized is supported by acoustic emission monitored experiments on uniaxial tensile loaded isotropic paper sheets.

As can be seen in Fig. 10 does the exponential damage evolution law capture the descending part reasonable well and this lends confidence to the chosen model.

7. Verification of the model

Of particular interest is transferability, i.e. that one set of model parameters can describe the mechanical behavior of significantly different geometries. Experiments, as well as numerical analyses, have been made using specimens III and IV (illustrated in Fig. 11) in order to investigate the transferability.

The boundary conditions are as in Eqs. (45) and (46). The finite element meshes for specimens III and IV are as shown in Fig. 12.

In all the computations the material is modeled as an orthotropic material with an elastic–plastic yield criterion (Eq. (16)) and a damage criterion (Eq. (31)). The material parameters are as presented in Tables 1–3 and an exponential damage evolution law is utilized (Eq. (39)). The specimens, both in Kraftliner and Testliner, are loaded in MD and CD.

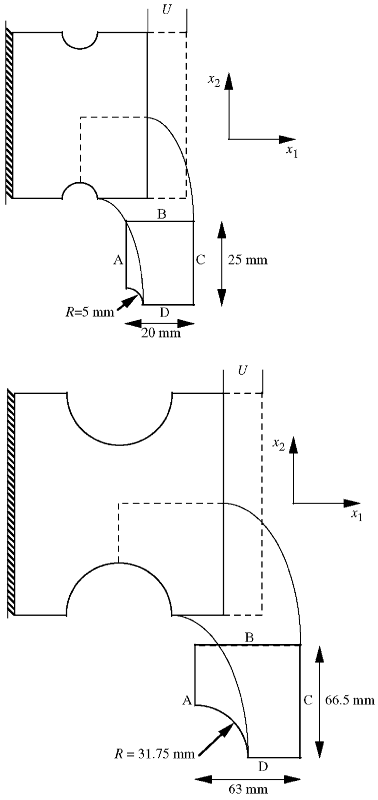

Fig. 11. Schematic representation of portions of modeled specimens III and IV.

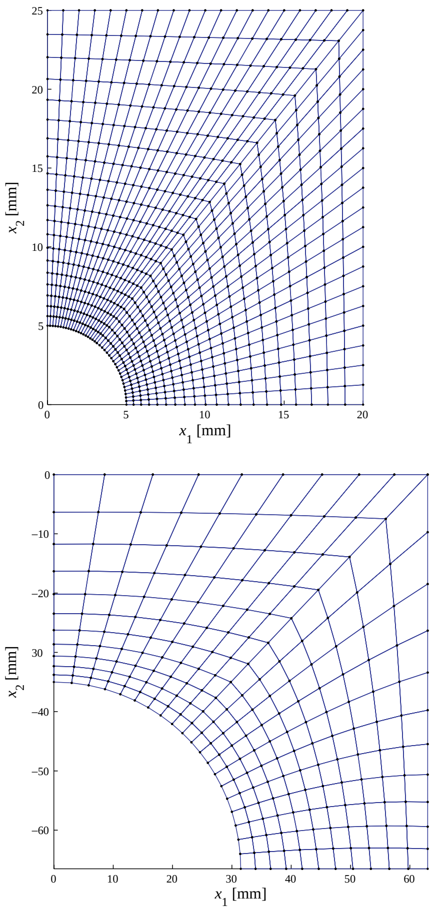

Fig. 12. Meshes consisting of 800 (specimen III) and 220 (specimen IV) elements, respectively.

7.1. Analysis of results

Fig. 13 presents computed load–elongation curves together with experimentally obtained curves for the discussed specimens, materials and loading directions. In each plot, the four cases belonging to the same material are displayed. Also displayed are the computed loads for onset of damage growth marked.

The exponential damage evolution law used seems to describe almost entirely correct the descending part of the load–elongation curves. As can be seen in Fig. 13, the numerically obtained and the experimentally measured load–elongation curves show good agreement.

From now on, we restrict the presented results to specimen III only. The results obtained in analyses on specimen IV are similar and, for the sake of clarity, excluded in the following discussion.

Fig. 14 show typical damage distributions in specimen III calculated for the considered loading cases. The damage component displayed is the largest of D_1 and D_2. The plots presented in Fig. 14 are contour plots showing the damage at the load step when the first element becomes fully damaged ($=$onset of breakage), i.e. when $\max\{D_1, D_2\} \to 1$. Note that only contour lines corresponding to damage levels of 0.2, 0.5 and 0.8 are shown.

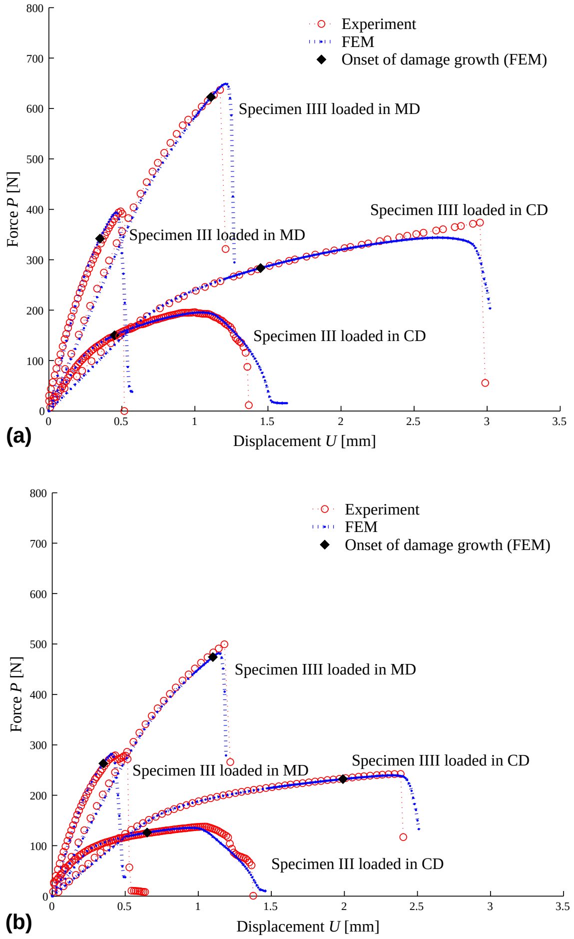

Fig. 13. Load–elongation plots for specimens III and IV. The numerical results are displayed together with experimentally obtained values. Kraftliner (a) and Testliner (b).

It can also be noted in Fig. 14 that the damage is more concentrated to the interior of specimen III when the specimen is loaded in CD than in MD. When the specimen is loaded in MD, the highest level of damage is located close to the boundary of the notches, whereas when the specimen is loaded in CD the highest levels of damage is located at about 1/2 mm (Kraftliner) and 1 mm (Testliner) from the notch boundary.

Fig. 15 shows computed damage evolutions at the point in the material that exhibits the highest level of damage for respective loading case. The results are calculated at different locations in the modeled geometry, depending on loading direction and paper material, according to Fig. 14.

When the specimen is loaded in CD is $\max\{D_1\} \geqslant \max\{D_2\}$, whereas the opposite holds when the specimen is loaded in MD. Hence, if damage growth has occurred, the computed levels of damage are always equal or higher in the cross-direction of the material than in the machine direction, independently of loading direction.

To illustrate the problem of localization, a comparison of the total damage growth of D_1 when $l = 0$ and $l = 2$ when utilizing two different mesh densities is shown in Fig. 16. In this particular case is a Kraftliner loaded in CD until complete breakage. As indicated in Fig. 16, mesh refinement leads to localized

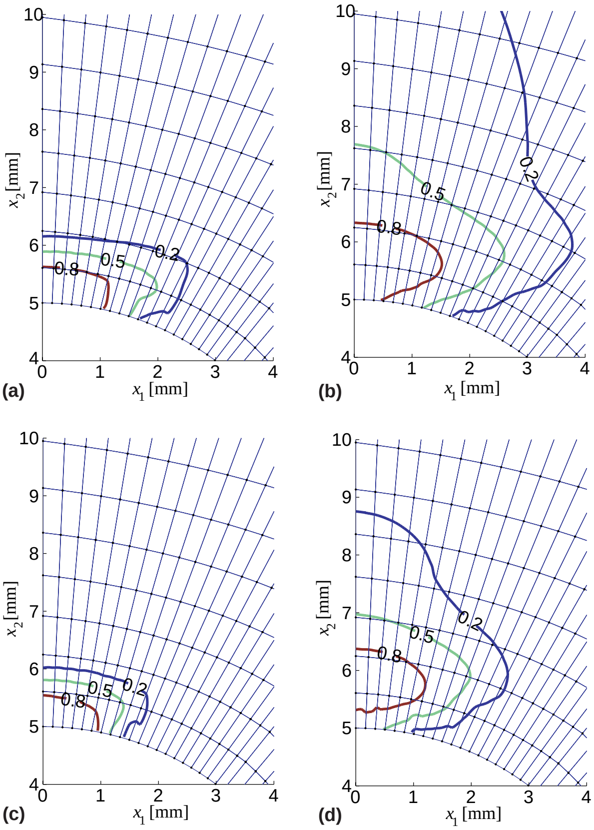

Fig. 14. Damage contours immediately before onset of breakage of specimen III. Kraftliner loaded in MD (a) and CD (b). Testliner loaded in MD (c) and CD (d).

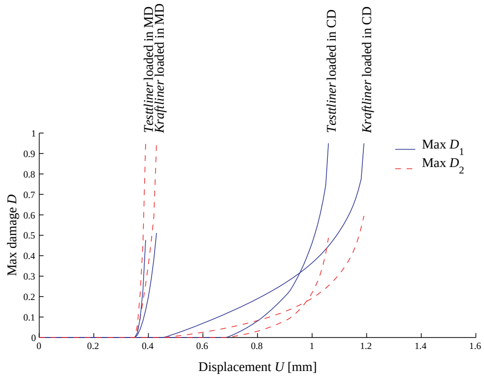

Fig. 15. Damage evolution history in specimen III during loading. Note that the presented results are computed at different locations in the geometry, depending on loading direction and material.

deformation in a region of decreasing volume along the x_2-axis. When the gradient enhanced approach is adapted, i.e. $l > 0$, this problem is avoided. The region of localization is stretched over several elements and the density of the finite element mesh is not crucial.

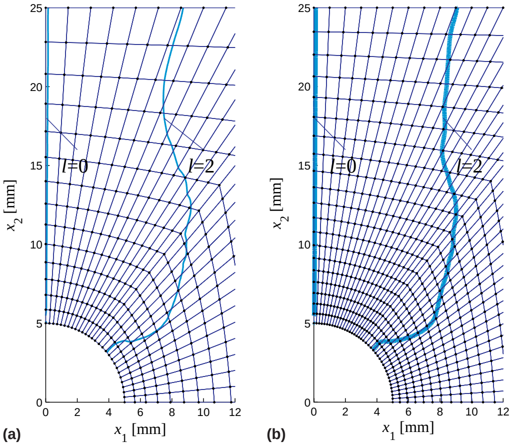

Fig. 16. Damage contours at complete breakage of specimen III. Kraftliner loaded in CD. Only contour lines corresponding to $D_1 \geqslant 0.95$ are displayed. Mesh consisting of 392 elements (a) and mesh consisting of 800 elements (b).

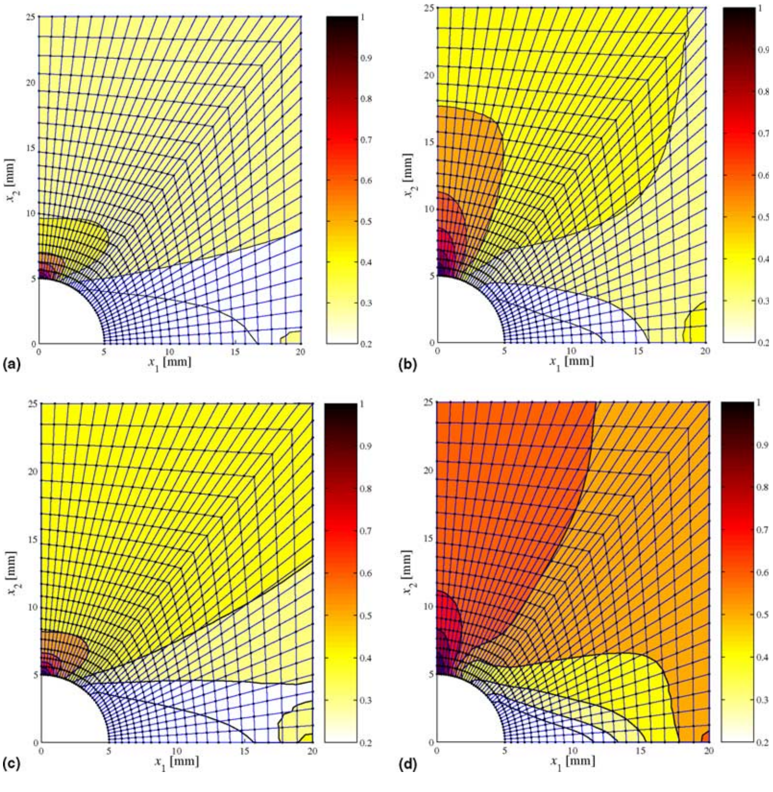

Fig. 17. Relative equivalent stress contours immediately before breakage of specimen III. As the area is darker the stress is higher. Kraftliner loaded in MD (a) and CD (b). Testliner loaded in MD (c) and CD (d).

In Fig. 17 are the relative Hill equivalent stress $\hat{\sigma}_e / \max\{\hat{\sigma}_e\}$ contours displayed for the same cases as in Fig. 14. The highest concentration of equivalent stress $\hat{\sigma}_e$ is located immediately at the notch boundaries in the specimens. However, when the specimen is loaded in CD, the region with the highest equivalent stress concentration is larger in size and concentrated to a narrow band around $x_1 = 0$ along the x_2-axis.

When the specimen is loaded in MD, the region with the highest concentration of equivalent stress $\hat{\sigma}_e$ is located at the notch boundaries and concentrated to a smaller region in comparison to when the specimen is loaded in CD. It is worth noticing that the plastic strains are relatively larger in the interior of the specimen when it is loaded in CD as compared to when the it is loaded in MD. This may have consequences for the subsequent crack nucleation that has been observed in the experiments, as high density of plastic strains is detrimental to the integrity of the specimen.

8. Conclusions

The mechanical behavior of two packaging paper materials subjected to tensile loading up to complete breakage has been studied.

A model for isotropic strain hardening elastic anisotropic plasticity, coupled to anisotropic damage, is discussed. The model has been analyzed in a non-linear finite element procedure.

The constitutive relations, including a gradient enhanced damage model, are developed within a thermodynamical framework and the Helmholtz free energy in the continuum is assumed to depend not only on the strain and stress components but also on the damage in the material.

The following conclusions are made:

- The capability of the model to properly capture and simulate the damage mechanism of a paper material is demonstrated by means of several numerical examples which are compared to, and verified with, experiments on paper specimens of varying geometry.
- The results demonstrate the ability of the model to model irreversible deformations up to complete breakage of tensile loaded paper specimens.
- The model can be calibrated using load–elongation curves obtained from tensile testing.
- The exponential damage evolution law utilized seems to describe the descending part of load–elongation curves reasonable well.
- The density of the finite element mesh is not crucial as an introduction of a material characteristic length fixes the width of the zone in which damage localizes, thus preventing strain localization into a vanishingly small region with zero energy dissipation.
- The results indicate that a characteristic length parameter in a gradient enhanced approach can be related to the average fibre length in a paper material. It has been found that a value of l equals approximate $l \approx 2l_f$ where l_f is the average fibre length, generates reasonable correspondence between the experiments and the numerical analysis.

Acknowledgements

Financial support from Bo Rydin Foundation and the 5th framework program of EU (QLK5-CT-2002-00772 AEP) is gratefully acknowledged. Finally, the authors are grateful to an anonymous reviewer for valuable comments that greatly improved the manuscript.

References

Bathe, K.J., 1982. Finite Element Procedures in Engineering Analysis. Prentice-Hall, NJ, USA.

Baum, G.A., Brennan, D.C., Habeger, C.C., 1981. Orthotropic elastic constants of paper. Tappi 64, 97–101.

Chow, C.L., Wang, J., 1987. Anisotropic theory of continuum damage mechanics for ductile fracture. Eng. Fract. Mech. 27, 547–558.

Comi, C., 2001. A non-local model with tension and compression damage mechanics. Eur. J. Mech. A/Solids 20, 1–22.

Contrafatto, L., Cuomo, M., 2002. A new thermodynamically consistent continuum model for hardening plasticity coupled with damage. Int. J. Solids Struct. 39, 6241–6271.

Cook, R.D., Malkus, D.S., Plesha, M.E., 1989. Concepts and Applications of Finite Element Analysis. John Wiley & Sons, Singapore.

Cordebois, J.P., Sidoroff, F., 1982. Damage induced elastic anisotropy. In: Boehler, J.P. (Ed.), Mechanical Behaviour of Anisotropic Materials. CNRS, Paris, France.

de Borst, R., Pamin, J., Geers, M.G.D., 1999. On coupled gradient-dependent plasticity and damage theories with a view to localization analysis. Eur. J. Mech. A/Solids 18, 939–962.

Engelen, R.A.B., Geers, M.G.D., Baaijens, F.P.T., 2003. Nonlocal implicit gradient-enhanced elasto-plasticity for the modelling of softening behaviour. Int. J. Plasticity 19, 403–433.

Eringen, A.C., Edelen, D.G.B., 1972. On nonlocal elasticity. Int. J. Eng. Sci. 10, 233–248.

Ganghoffer, J.F., de Borst, R., 2000. A new framework in nonlocal mechanics. Int. J. Eng. Sci. 38, 453–486.

Geers, M.G.D., 1997. Experimental analysis and computational modelling of damage and fracture. Ph.D. Thesis. Eindhoven University of Technology, The Netherlands.

Gradin, P., Nyström, S., Flink, P., Forsberg, S., Stollmaier, F., 1997. Acoustic emission monitoring of light-weight coated paper. J. Pulp Paper Sci. 23, 113–118.

Gradin, P., Isaksson, P., submitted. The onset and progression of damage in an isotropic paper sheet.

Hansen, N.R., Schreyer, H.L., 1994. A thermodynamically consistent framework for theories of elastoplasticity coupled with damage. Int. J. Solids Struct. 31, 359–389.

Hill, R., 1950. The Mathematical Theory of Plasticity. Clarendon Press, Oxford UK.

Ju, J.W., 1989. On energy-based coupled elastoplastic damage theories: constitutive modelling and computational aspects. Int.J. Solids Struct. 25, 803–833.

Kachanov, L.M., 1958. Time of the rupture process under creep condition. Izv. Akad. Nauk SSSR, Otd. Tekhn. Nauk 26-31, 1958 (in Russian).

Kröner, E., 1967. Elasticity theory of materials with long range cohesive forces. Int. J. Solids Struct. 3, 731–742.

Kuhl, E., Ramm, E., 1999. Simulation of strain localization with gradient enhanced damage models. Comput. Mater. Sci. 16, 176–185.

Kuhl, E., Ramm, E., de Borst, R., 2000. An anisotropic gradient damage model for quasi-brittle materials. Comput. Methods Appl. Mech. Eng. 183, 87–103.

Lasry, D., Belytschko, T., 1988. Localization limiters in transient problems. Int. J. Solids Struct. 24, 581–597.

Lemaitre, J., 1985. Coupled elastoplasticity and damage constitutive equations. J. Comput. Methods Appl. Mech. 51, 31–49.

Lemaitre, J., Chaboche, J.L., 1990. Mechanics of Solid Materials. Cambridge University Press, Cambridge, UK.

Matlab, 2002. Version 6.5. The MathWorks Inc., Natick, MA, USA.

Maugin, G.A., 1992. The Thermomechanics of Plasticity and Fracture. Cambridge University Press, UK.

Mühlhaus, H.-B., Aifantis, E.C., 1991. A variational principle for gradient plasticity. Int. J. Solids Struct. 28, 845–857.

Niskanen, K., Kettunen, H., Yu, Y., 2001. Damage width: a measure of the size of fracture process zone. In: 12th Fundamental Research Symposium, Oxford, UK.

Pijaudier-Cabot, G., Bazant, Z.P., 1987. Nonlocal damage theory. J. Eng. Mech. 113, 1512–1533.

Peerlings, R.H.J., de Borst, R., Brekelmans, W.A.M., de Vree, J.H.P., 1996. Gradient enhanced damage for quasi-brittle materials. Int. J. Numer. Methods Eng. 39, 3391–3403.

Peerlings, R.H.J., Brekelmans, W.A.M., de Borst, R., Geers, M.G.D., 2000. Enhanced damage modelling of quasi-brittle and fatigue fracture—computational aspects. In: Proceedings of the European Congress on Computational Methods in Applied Sciences and Engineering, incorporating the VI International Conference on Computational Plasticity (COMPLAS VI); Barcelona, Spain, 11–14 September, pp. 1–20.

Simo, J.C., Ju, J.W., 1987. Strain and stress-based continuum damage models—I. Formulation. Int. J. Solids Struct. 23, 821–840.

Steinmann, P., Carol, I., 1998. A framework for geometrically nonlinear continuum damage mechanics. Int. J. Eng. Sci. 36, 1793–1814.

Szilard, R., 1974. Theory and Analysis of Plates. Prentice-Hall, NJ, USA.

Tryding, J., 1996. In-plane fracture of paper. Ph.D. Thesis. Division of Structural Mechanics, Lund University, Sweden.

Voyiadjis, G.Z., Kattan, P.I., 1992. A plasticity-damage theory for large deformations of solids. Part I: Theoretical formulation. Int. J. Eng. Sci. 30, 1089–1108.

Voyiadjis, G.Z., Park, T., 1997. Anisotropic damage effect tensors for the symmetrization of the effective stress tensor. J. Appl. Mech. 64, 106–110.

Xia, Q.S., Boyce, M.C., Parks, D.M., 2002. A constitutive model for the anisotropic elastic–plastic deformation of paper and paperboard. Int. J. Solids Struct. 39, 4053–4071.

Zhu, Y.Y., Cescotto, S., 1995. A fully coupled elasto-visco-plastic damage theory for anisotropic materials. Int.J. Solids Struct. 32, 1607–1641.